Nanoscale Res Lett (2007) 2:94–99
DOI 10.1007/s11671-006-9036-2

NANO EXPRESS

Tunable self-assembly of one-dimensional nanostructures with orthogonal directions

Milan P. Allan · Simon Berner · Martina Corso · Thomas Greber · Jürg Osterwalder

Published online: 26 January 2007

Abstract High-temperature exposure of a Mo(110) surface to borazine $(HBNH)_3$ leads to the formation of two distinctly different self-assembling nanostructures. Depending on the substrate temperature during preparation, either well-aligned, ultra-thin boron nanowires or a single-layer stripe structure of hexagonal boron nitride forms. Both structures show one-dimensional (1D) characteristics, but in directions perpendicular to each other. It is also possible to grow the two phases in coexistence. The relative weights are controlled by the sample temperature during preparation.

Keywords Hexagonal boron nitride (*h*-BN) · Boron · One-dimensional nanostructures · Nanowire · Photoemission · Scanning tunneling microscopy (STM) · Low energy electron diffraction (LEED)

In nanoscience and nanotechnology, there is an ubiquitous need for arranging nanometer-sized objects on surfaces in an orderly way. The atomic lattices of stable inorganic materials are usually too narrowly spaced for such applications, and research has focused on surface-superstructures with periodicities in the one to a few nanometer range, which can serve as templates e.g., for the formation of ordered layers of well-separated molecules, or for the growth of ordered metallic deposits and monodisperse metallic clusters [1]. One-dimensional (1D) superstructures represent an important class of templates, with confining potentials for electrons, molecules or metallic adsorbates along one direction parallel to the surface. Examples for 1D superstructures on surfaces include vicinal surfaces [2, 3] submonolayer oxygen adsorbate structures on Cu(110) [4] or submonolayer structures of larger molecules organized into stripes by long-range, substrate-mediated interaction [5]. However, these 1D templates are often not very stable and not well ordered on a micrometer scale.

Monolayer structures of hexagonal boron nitride (*h*-BN) on transition metal surfaces have received much interest recently. On Ni(111), which has a lattice spacing that is nearly equal to that of *h*-BN (2.49 Å for nickel, 2.50 Å for *h*-BN), the chemical vapor deposition (CVD) of benzene-like borazine $(HBNH)_3$ at 1050 K leads to very uniform epitaxial monolayers [6]. On Rh(111) the large lattice mismatch causes the *h*-BN to form a highly ordered mesh-like nanostructure with a periodicity of about 3 nm: the *nanomesh* [7]. On Pd(110) and Pd(111), where the lattice mismatch is even larger, continuous single-layer films are observed that exhibit a variety of moiré patterns [8, 9]. A common aspect of these boron nitride layers is that, as a result of the high preparation temperatures, they represent chemically inert and highly temperature-resistant nanotemplates for the production of ordered molecular films or monodisperse metal clusters. It would thus be desirable to have also 1D templates based on this material.

In this letter, we report two new self-assembling nanostructures grown by high-temperature CVD of borazine on the (110) surface of bcc molybdenum. This surface has a centered rectangular structure that is nearly but not quite hexagonal, and should thus be an interesting template for growing hexagonal boron

M. P. Allan · S. Berner · M. Corso · T. Greber · J. Osterwalder (✉)
Physik-Institut, Universität Zürich, Winterthurerstrasse 190, 8057 Zurich, Switzerland
e-mail: osterwal@physik.unizh.ch

nitride layers. It is anisotropic with lattice spacings of 3.15 Å ([001] direction), 4.45 Å ([1–10]) and 2.64 Å ([1–11]). This property reflects itself in the 1D character of the arising structures: depending on the temperature of the sample during preparation, a striped *h*-BN phase, a boron nanowire (BNW) phase, or a coexistence of the two are observed. Both phases have 1D characteristics, but in directions perpendicular to each other. Furthermore, the area ratio of the two phases can easily be tuned by varying the preparation temperature. The two phases will be presented separately, followed by a discussion about the coexistence regime and the temperature dependence of the phase distribution.

All experiments were performed in an ultra-high-vacuum system (described in Ref. [10]) equipped with instrumentation for ultra-violet photoelectron spectroscopy (UPS), angle-resolved photoelectron spectroscopy (ARPES), X-ray photoelectron spectroscopy (XPS), X-ray photoelectron diffraction (XPD), low-energy electron diffraction (LEED) and scanning tunneling microscopy (STM). The data shown in the figures were recorded at room temperature. The molybdenum single crystal was cleaned by a process adapted from the literature [11]. The process consists of oxygen exposure followed by high temperature (2200 K) flashing. The cleanliness was tested by LEED, UPS, and XPS; contamination levels were below the detection limit of 5% of a monolayer (one monolayer is taken to be 1.42×10^{15} atoms cm^{-2}, equal to the Mo(110) surface atom density). The sample surface temperature was measured by an optical pyrometer. Its relative accuracy is estimated to be better than 30 K, its absolute accuracy to about 80 K. The CVD process was conducted similar to Ref. [6]: borazine vapor is inserted into the chamber through a leak valve connected to a glass tube containing liquid borazine. In the chamber, it reacts with the hot substrate surface under release of H_2 to create the *h*-BN layers. The sample is exposed to 3×10^{-7} mbar of borazine vapor for 3 min (equal to 41 Langmuir) at a given sample surface temperature, followed by one minute of post-annealing. The preparation temperature was varied between 950 K and 1170 K.

When the CVD of borazine is carried out at preparation temperatures of about 950 K, a graphene-like *h*-BN structure forms on the Mo(110) surface. It consists of a single *h*-BN layer and exhibits a 4×1 superstructure of the Mo(110) surface lattice. Note: We refer here to the centered rectangular lattice; the superstructure consists thus of a new periodicity of four times the Mo(110) lattice spacing along [001] and one time along [1–10] (Fig. 1 shows a model). The

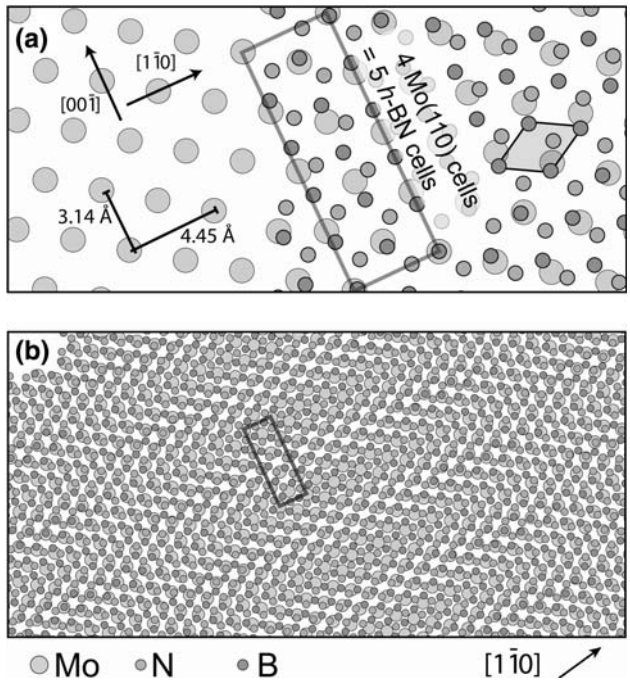

Fig. 1 (**a**) Simplified model of the centered rectangular Mo(110) surface (left) with the correctly oriented, but unstrained *h*-BN structure overlaid (right). The *rhombus* shows a 1×1 *h*-BN unit cell. The *rectangle* indicates the 4×1 superstructure of the Mo(110) surface lattice discussed in the text. Note that four substrate spacings match five *h*-BN spacings along the [001] direction, and 10 *h*-BN unit cells fit on 8 molybdenum surface atoms. (**b**) A larger area view. The stripes along the [1–10] direction are a moiré pattern. Note that all models, as well as STM, LEED and XPD images are oriented the same way throughout this letter

proposed structure can be deduced from XPD, ARPES, and LEED measurements: XPD data are similar to those of *h*-BN on Ni(111) [12] and establish the single-layer quality and the flatness of the structure. ARPES data, presented in Fig. 2 show σ- and π-bands in the binding energy region from 5 to 12 eV, as measured and calculated previously for other *h*-BN monolayer structures [13]. The orientation of the *h*-BN layer with respect to the substrate was obtained by a procedure based on the anisotropy of the band structure, which is described in Ref. [14]. The result is shown in the simplified model depicted in Fig. 1, which shows an unstrained *h*-BN layer on top of the Mo(110) surface. From the extra spots in the LEED pattern (Fig. 3b, inset), a 4×1 superstructure containing eight molybdenum surface atoms and 10 *h*-BN unit cells can be deduced. This is supported by consideration of the lattice spacings: along [001], four substrate spacings match five *h*-BN spacings, with a lattice mismatch $M^{[001]} = (5\, a^{[001]}_{overlayer} - 4\, a^{[001]}_{substrate})/4\, a^{[001]}_{substrate}$ of only –0.6%. Along the [1–10] direction, the lattice mismatch is $M^{[1-10]} = -2.6\%$. The super-

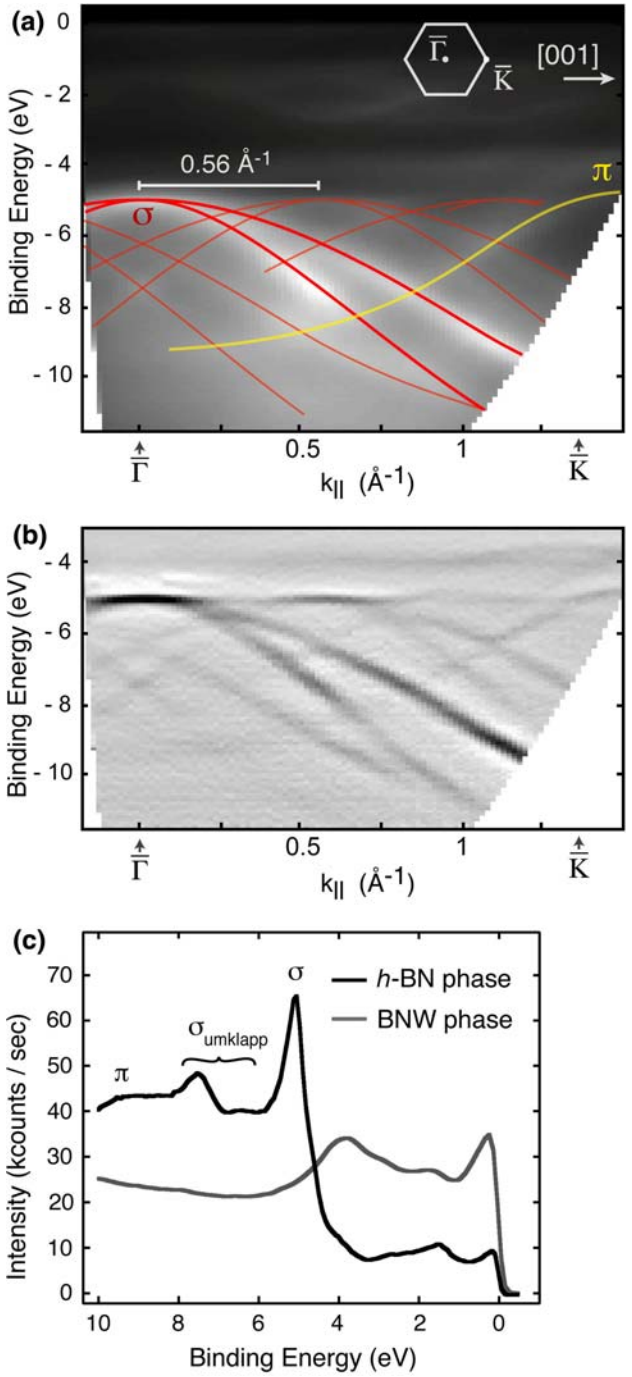

Fig. 2 (**a**) The ARPES data measured along the [1–10] direction. Photoelectron intensities are plotted in grey scale. The *hexagon* shows the Brillouin zone and defines characteristic points. The *thick red and yellow lines* mark the σ– and π–band, respectively; the *thin red lines* indicate umklapp bands, i.e., σ–bands shifted by a reciprocal lattice vector in agreement with the proposed superstructure. (**b**) The same data as in (**a**), but the second derivative with respect to the binding energy is plotted in order to enhance the visibility of the bands. In (**c**), we give the UPS normal emission spectrum, and for comparison the one from the boron (BNW) phase (see below)

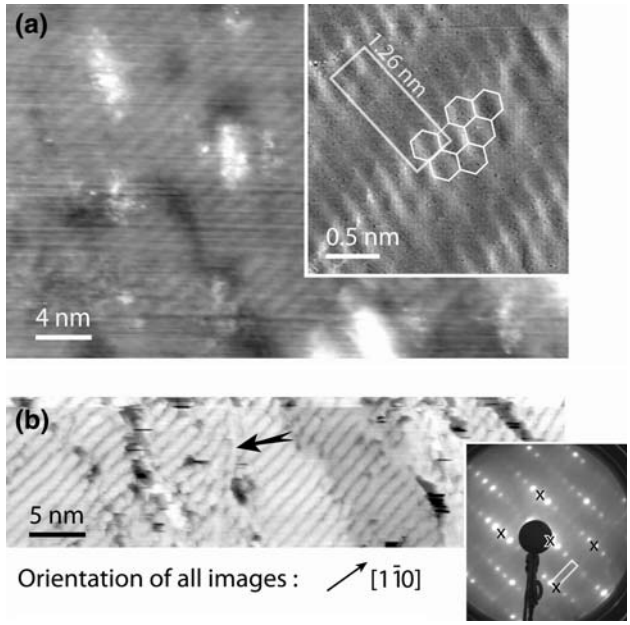

Fig. 3 (**a**) Stripes with a periodicity of 1.26 nm are clearly visible in STM images of the *h*-BN phase. (The image was taken with a bias voltage of $V_B = 1.8$ V and a set tunneling current of $I_T = 1$ nA.) The corrugation in STM images of the *h*-BN phase varies between 0.6 and 1.6 Å, most likely due to different tip conditions. The inset shows a small area measurement (current image, $V_B = 1$ V, $I_{T\,set} = 10$ nA). *White hexagons* indicate a part of the *h*-BN lattice drawn in the correct size and orientation from the proposed model. The *rectangle* underlines the 4×1 superstructure (cf. Fig. 1). (**b**) A squeezing and twisting of the stripes (*arrow*) occurs at some places ($V_B = -3$ V, $I_T = 0.6$ nA). The inset shows the LEED pattern recorded from the same preparation. The markers indicate the integer spots of the molybdenum substrate. The unit cell of the superstructure described in the text is shown by the white rectangle

structure is not only visible in the geometric structure (measured by LEED) but also in the electronic structure: In the ARPES data of Fig. 2, dim replica of the original *h*-BN bands are visible, shifted by ca. 0.56 $Å^{-1}$. These so-called umklapp bands come from the new periodicity of five *h*-BN lattice spacings, which equal four substrate spacings.

STM images show clear stripes along the [1–10] direction (Fig. 2). The spacing between the stripes corresponds to four molybdenum spacings, i.e., 1.26 nm. Such patterns on STM images can stem from real topographic structures or from a moiré pattern, as observed on *h*-BN/Pd(111) [9]. The latter case is illustrated in Fig. 1. However, in the case discussed here, we have indications that the stripes are topographic in nature, i.e., that the *h*-BN layer is broken up, since the stripes are sometimes twisted and bent. The structural disorder necessary to produce such a bend in a moiré pattern is unlikely to occur.

The lattice mismatch along the [1–10] direction is $M^{[1-10]} = -2.6$ %. Surprisingly, we do not see the specific periodic modulations along the stripes, which we would expect for a moiré pattern. Those should have a periodicity of about 17 nm. Most of the stripes have a length that is considerably shorter than this periodicity, due to the presence of a high defect density. It was not possible to grow this striped *h*-BN phase with lower defect density, presumably due to the competition with the higher temperature boron phase (see below).

If the borazine exposure, as described above, is conducted with the sample surface held at higher preparation temperature (1170 K), a very different phase appears: a nanostructure consisting of B nanowires (*BNW phase*). STM images (Fig. 3) display extremely well-aligned wires. XPS analysis shows that all nitrogen has disappeared during preparation; the structure is thus purely boron or a boron molybdenum phase. In recent years, boron was often found to form nanostructures: boron nanowires (amorphous or crystalline), ribbons and tubular structures [15] were created. Different from the ones described in this letter, the nanowires were freestanding and usually relatively thick (30–900 nm). The experimental activities in building and investigating boron nanostructures have been accompanied by theoretical activities. The electron deficient character of boron leads to high structural flexibility, and in fact, ab initio calculations predict a variety of boron structures to be stable, including layered, tubular and chain-like boron structures [15–18]. The BNWs that we observed on Mo(110) are 2–10 nm wide and up to 1 μm long (Fig. 4). This leads to extremely high aspect ratios of up to 500. Corrugation as seen by STM is around 4–6 Å, often in steps of 2 Å. LEED measurements show that the structure is perfectly periodic along the BNWs but not perpendicular to them. A reason for this might be structural disorder induced by boron atoms solved in the molybdenum crystal, as discussed below.

We performed X-ray photoelectron diffraction (XPD) measurements in order to obtain information about the local geometric structure of the BNWs. In this technique a core-level intensity, here it is B1s, is measured for many polar and azimuthal angles, it is chemically resolved. In the single scattering cluster (SSC) model, one assumes that the photoelectron is scattered only once at neighboring atoms. Since forward scattering usually dominates, intensity maxima appear on XPD angular plots at the directions of nearest neighbors. The interference of the emitted photoelectron waves with the waves scattered at neighboring atoms leads to interference rings centered at forward scattering directions, which give information about the distance from emitter to scatterer. A good introduction to XPD can be found in Ref. [19]. Typically one uses a trial and error procedure for structure determination with XPD, calculating simulated patterns for possible structures. For our analysis, we used a multiple scattering calculation code by P. Kaduwela et al. [20] going beyond single scattering up to 9th order.

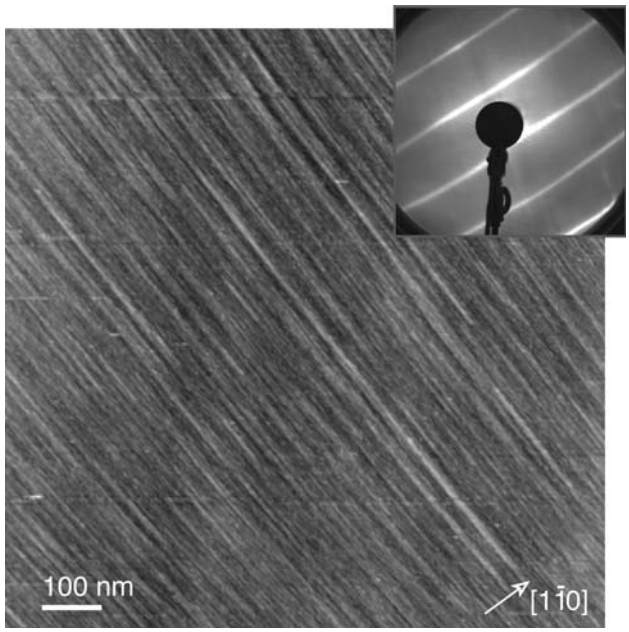

Fig. 4 STM image of the BNW phase (V_B = 1 V, I_T = 1 nA). Note that some BNWs cross the whole image. The corrugation is up to 6 Å. The inset shows a LEED image with the same orientation of the sample surface. It evidences that the structure is periodic along the wires, but not perpendicular to them

Our XPD data are depicted in Fig. 5a. Clear interference rings can be seen around forward scattering peaks along the [001] direction. The sharpness of the rings indicates long-range order along [001] and multiple scattering. We propose that the rings originate from a chain-like structure, from which a simulated pattern is depicted in Fig. 5c. The forward scattering peaks, however, may stem from interstitial boron atoms solved in the bulk at the octahedral positions of the Mo(110) lattice (Fig. 5b). More complex boron structures are also possible.

The XPS B1s core-level peak energy and shape should, in principle, give more information about the bonding of the boron atoms, since different chemical neighborhoods lead to *chemical shifts* in the core level binding energies. The B1s level is measured at a binding energy of 188.3 eV. It is, however, not straightforward to compare this value to reference data of pure boron or boron compounds with B–B bonds, since the latter are ambiguous [21]. Values reaching from 186.5 to 188.5 eV

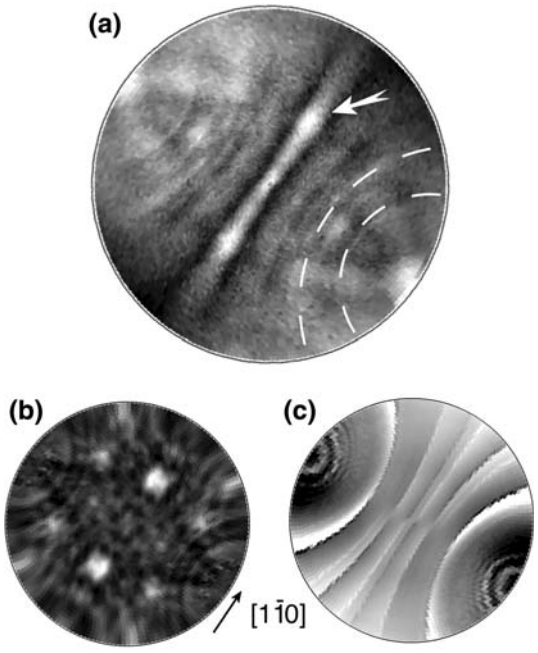

Fig. 5 (**a**) Stereographically plotted XPD measurements of the B1s core level, with normal emission in the centre and 90° polar angle at the outer ring. Intensities are given in a grey scale. The kinetic energy of the electrons is 1,065.2 eV. Note the forward scattering peaks (one is marked by the *arrow*) and the interference rings (some highlighted by *dashed white lines*). (**b**) A simulated pattern from boron atoms solved in the octahedral positions of the molybdenum crystal. (**c**) The same, but for a boron chain with interatomic distance = 1.05 Å, which is one third of the molybdenum spacing. The distance *d* was varied to produce an optimal fit to the interference fringes in the data of (**a**)

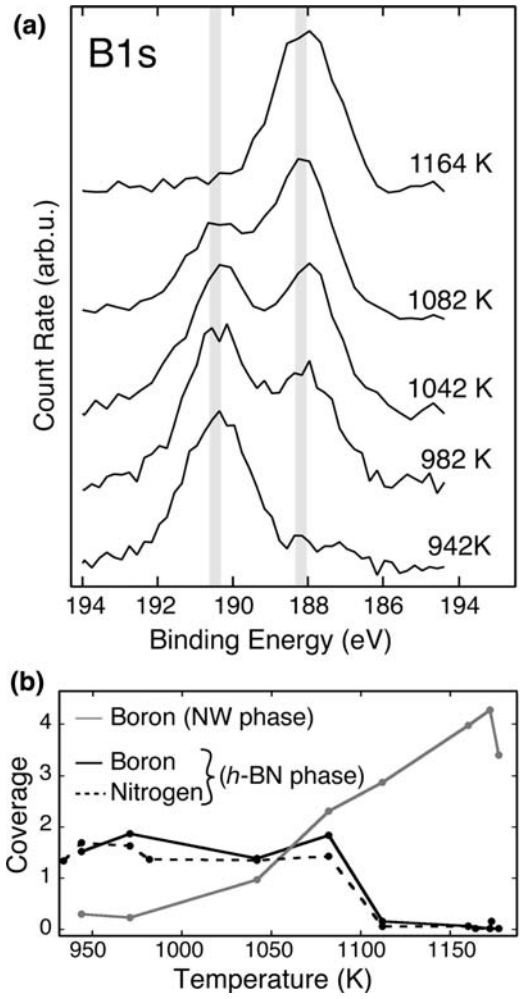

Fig. 6 (**a**) Temperature dependence of the B1s XPS spectra. The preparation temperatures are indicated on the right hand side. The double peak represents the two chemical states of the boron in the two-phase region. (**b**) The coverages of nitrogen and boron, the latter resolved in the two phases, plotted versus the preparation temperature. The coverage of boron in the *h*-BN follows, as expected, the coverage of nitrogen. The abundances of the two phases change gradually

can be found in the literature [22–24]. But one can say that the boron atoms in the BNW phase must have chemical surroundings very different from the boron atoms in the *h*-BN structure described above, since there is a chemical shift of 2.4 eV between the two structures (Fig. 6a).

After having discussed the pure *h*-BN and BNW phases, the question arises as to what happens if one prepares the sample at intermediate preparation temperature. We will start our discussion with the results from XPS measurements. As mentioned already, there is a large chemical shift in the B1s core-level energies. For samples prepared at intermediate temperatures, a double peak is visible in the B1s XPS spectra, representing the two chemical states of the boron. With varying preparation temperature, the peaks change neither their positions nor widths, but only their relative intensities (Fig. 6a). This is a strong indication that no new kind of structure forms at intermediate preparation temperatures, but that the two phases coexist. Further proof comes from XPD measurements: the double peak in the B1s XPS spectrum allows to simultaneously take two XPD scans at the respective peak energies of the two phases. This way one can distinguish between the local structures of the boron in the BNW phase and the boron in the *h*-BN phase. These XPD data (not shown) confirm that the two phases coexist on surfaces prepared at intermediate temperatures.

The coverages of nitrogen and boron, resolved in the two phases, versus the preparation temperature can be extracted from the integrated signals of the XPS B1s and N1s peaks (Fig. 6b). The quantities change gradually with increasing preparation temperature from the *h*-BN to the BNW phase. This holds also for LEED, UPS and STM measurements. The UPS spectrum of the BNW phase is shown in Fig. 2c in comparison with the one from the striped *h*-BN phase.

The change from low- to high-temperature phase can not only be observed when increasing the preparation temperature but also simply by annealing the low-temperature *h*-BN phase. An experiment was carried out by subsequent annealing of the sample followed by checking the structure with XPS. The high-temperature phase was identified by the characteristic LEED pattern and the B1s peak energy. During annealing, no boron is leaving the surface. The overall amount of boron stays constant since there is neither a further boron source. Therefore the amount of boron is lower after this procedure than what is usually observed for the high temperature phase (cf. Fig. 6). Compared to the gradual change observed when increasing the preparation temperature, the phase transformation is here abrupt. It takes place between 1140 and 1240 K. No data points were recorded between these temperatures, thus the temperature range might be even narrower.

In summary, we report the discovery of a tunable system of two self-assembling nanostructures. The structures are very appealing because of their 1D characters and their directional orthogonality. The BNWs are extremely thin and long, leading to aspect ratios of up to 500. The 1D character, the easy preparation procedure, the homogeneity of the structure, and the high thermal stability opens possibilities for technological uses. The structures may be used as templates to create other 1D nanostructures, or to order and align nanoparticles such as molecules and atomic clusters. The latter is of great interest since the ordering of larger molecules is a crucial challenge in different fields, e.g., in molecular electronics or in biology. For carbon nanotubes e.g., many methods relay on photolithography. The boron nanowires could act as a template to align nanotubes from a solution, similar to the experiments of Ref. [25] but with higher densities. More specifically, the BNW phase might be useful to immobilize molecules in a highly ordered state after photoalignment, a recently discovered method suitable for a variety of molecules [26].

Since changing the preparation temperature allows to tune precisely the relative weights of the two phases, one can control the process of self-assembly, which might help to understand it. The possibility to change irreversibly from the low-temperature phase to the high-temperature phase by annealing might also have applications: local heating of parts of the surface, e.g., with a highly focused laser beam or an AFM tip, might be used to 'write' a conducting structure (BNW) within an insulating one (*h*-BN). This could be used to build very robust read-only, non-volatile memory.

Acknowledgment The authors would like to thank Martin Klöckner and Erwin Fischer (Eidgenössische Technische Hochschule Zürich) for technical support, Hermann Sachdev (Universität des Saarlandes) for the production of borazine, and Martin Morscher, Matthias Hengsberger, Anna Tamai and Jörg Kröger (Christian-Albrechts-Universität zu Kiel) for fruitful discussions. This work was supported by the Swiss National Science Foundation (SNF) and by the European Union's Sixth Framework Programme via the NanoMesh project (NMP4-CT-2004–013817).

References

1. J.V. Barth, G. Costantini, K. Kern, Nature. **437**, 671 (2005)
2. A. Tamai, W. Auwärter, C. Cepek, F. Baumberger, T. Greber, J. Osterwalder, Surf. Sci. **566**, 633 (2004)
3. F.J. Himpsel, A. Kirakosian, J.N. Crain, J.-L. Lin, D.Y. Petrovykh, Solid State Commun. **117**, 149 (2001)
4. K. Kern, H. Niehus, A. Schatz, P. Zeppenfeld, J. George, G. Comsa, Phys. Rev. Lett. **67**, 855 (1991)
5. S. Lukas, G. Witte, Ch. Woell, Phys. Rev. Lett. **88**, 028301 (2002)
6. A. Nagashima, N. Tejima, Y. Gamou, T. Kawai, C. Oshima, Phys. Rev. Lett. **75**, 3918 (1995)
7. M. Corso, W. Auwärter, M. Muntwiler, A. Tamai, T. Greber, J. Osterwalder, Science. **303**, 217 (2004)
8. M. Corso, T. Greber, J. Osterwalder, Surf. Sci. **577**, L78 (2005)
9. M. Morscher, M. Corso, T. Greber, J. Osterwalder, Surf. Sci. **600**, 3280 (2006)
10. T. Greber, O. Raetzo, T.J. Kreutz, P. Schwaller, W. Deichmann, E. Wetli, J. Osterwalder, Rev. Sci. Instrum. **68**, 4549 (1997)
11. J. Kröger, T. Greber, J. Osterwalder, Phys. Rev. B. **61**, 14146 (2000)
12. W. Auwärter, T.J. Kreutz, T. Greber, J. Osterwalder, Surf. Sci. **429**, 229 (1999)
13. G. Grad, P. Blaha, K. Schwarz, W. Auwärter, T. Greber, Phys. Rev. B. **68**, 085404 (2003)
14. T. Greber, L. Brandenberger, M. Corso, A. Tamai, J. Osterwalder, e-J. Surf. Sci. Nanotech. **4**, 410 (2006)
15. A. Quandt, I. Boustani, ChemPhysChem. **6**, 2001 (2005)
16. L. Seongbok, D.M. Bylander, L. Kleinman, Phys. Rev. B **42**, 1316 (1990)
17. M.K. Sabra, I. Boustani, Europhys. Lett. **42**, 611 (1998)
18. M.H. Evans, J.D. Joannopoulos, S.T. Pantelides, Phys. Rev. B **72**, 045434 (2005)
19. J. Osterwalder, P. Aebi, R. Fasel, D. Naumovic, P. Schwaller, T. Kreutz, L. Schlapbach, T. Abukawa, S. Kono, Surf. Sci. **333**, 1002 (1995)
20. A.P. Kaduwela, D.J. Friedman, C.S. Fadley, J. Electron Spectrosc. Relat Phenom. **57**, 223 (1991)
21. C.J. Powell, Appl. Surf. Sci. **89**, 141 (1995)
22. J.A. Schreifels, P.C. Maybury, W.E. Swartz, J. Catal. **65**, 195 (1980)
23. C. Ronning, D. Schwen, S. Eyhusen, U. Vetter, H. Hofsass, Surf. Coat. Technol. **158**, 382 (2002)
24. G. Takashi, H. Toshio, J. Mater. Sci. Lett. **7**, 548 (1988)
25. Y. Huang, X.F. Duan, Q.Q. Wei, C.M. Lieber, Science. **291**, 630 (2001)
26. M. Schadt, K. Schmitt, V. Kozinkov, V. Chigrinov, Jpn. J. Appl. Phys. **31**, 2155 (1992)